Geochemical Journal, Vol. 38, pp. 405 to 415, 2004

Si and Mg isotope fractionations in melilite in coarse-grained CAIs measured by SIMS

N. SUGIURA,* T. MIZUNO, T. USHIKUBO and H. HIYAGON

Department of Earth and Planetary Science, University of Tokyo, Tokyo 113-0033, Japan

(*Received August 25, 2003; Accepted March 2, 2004*)

Si and Mg isotopic compositions of melilite in three coarse-grained CAIs were measured by SIMS. Isotopic compositions of these elements were fractionated (1.0 to 2.9 ‰/amu for Si and 4.6 to 9.6 ‰/amu for Mg) relative to terrestrial values. These fractionations are similar to those reported for bulk CAIs (Clayton *et al*., 1988) and suggest that coarse-grained CAIs were formed by evaporative loss of some Si and Mg from high-temperature condensates as proposed by Grossman *et al*. (2000). No significant zoning of isotopic fractionations was observed in these CAIs. This suggests that the evaporative loss of these elements from CAIs were slow compared with diffusive homogenization and also suggests that evaporative loss ceased early before crystallization of Mg-rich melilite.

Keywords: CAI, Mg, Si, isotope fractionation, SIMS

INTRODUCTION

Si and Mg isotopic fractionations in coarse-grained calcium-aluminum-rich inclusions (CAIs) are indicators of evaporation processes experienced by CAIs (Clayton *et al*., 1988; Davis *et al*., 1990; Grossman *et al*., 2000). Si and Mg isotopic fractionations (up to ~5 ‰/amu for Si and ~11 ‰/amu for Mg) have been reported for bulk CAIs (Clayton *et al*., 1988 and references therein). Grossman *et al*. (2000) showed that most type B CAIs were depleted in Si and Mg relative to high-temperature condensates from the nebula and suggested that isotopic fractionations resulted from evaporative loss of these elements from condensates.

The model of Grossman *et al*. (2000) assumed that the temperature was constant during the evaporation event. A more detailed model was presented by Grossman *et al*. (2002) where the temperature was allowed to decrease while evaporation continued. Because of this continued evaporation, this model predicted that zoning of Si and Mg isotopic compositions should be observed in melilite (solid solution between akermanite ($Ca_2MgSi_2O_7$, Ak for short) and gehlenite ($Ca_2Al_2SiO_7$)) in CAIs.

Fairly large differences in Mg isotopic fractionations within individual CAI have been reported for several CAIs (Fahey *et al*., 1987; Davis *et al*., 1991; MacPherson and Davis, 1993; Goswami *et al*., 1994). Some CAIs show heavy isotope enrichment near the rim in accordance with the model by Grossman *et al*. (2002). Other CAIs, however, show opposite fractionation patterns, which require other processes such as recondensation and reequilibration. Homogeneous Mg isotopic fractionations in melilite mantle have been reported for two type B1 inclusions (MacPherson *et al*., 1989; Kennedy *et al*., 1997). Numerous data of Mg isotopic fractionations within a CAI were reported by MacPherson and Davis (1993), but the significance of the variation of the reported isotopic fractionation was not discussed. It is not known if Mg isotopic heterogeneity is common among CAIs.

Si isotopic fractionations, when measured together with Mg isotopic fractionation, may provide valuable information on the temperature during the evaporation process and also Si concentrations in the melt (Grossman *et al*., 2000). Reports of Si isotope fractionations measured by secondary ion mass spectrometry (SIMS) are rare (e.g., Davis *et al*., 1991; Clayton *et al*., 1984). Generally, measurements of small degrees of intrinsic isotope fractionations by SIMS are difficult because deviations of instrumental isotope fractionations (which are often quite large when measured by SIMS) cannot be separated from intrinsic isotope fractionations. Recent reports of Si isotope measurements (Hua *et al*., 2000, 2001a, 2001b) suggested that precise measurements were difficult.

Here we report Si and Mg isotope measurements of melilite in coarse-grained CAIs by SIMS. Our aims are 1) to establish a protocol for precise measurements of Si (and Mg) isotope fractionations and 2) to find out the degree of correlation between Si- and Mg-isotope fractionations in CAIs and 3) to find out if Si- and Mg-isotopic heterogeneity within CAIs are common.

*Corresponding author (e-mail: sugiura@eps.s.u-tokyo.ac.jp)

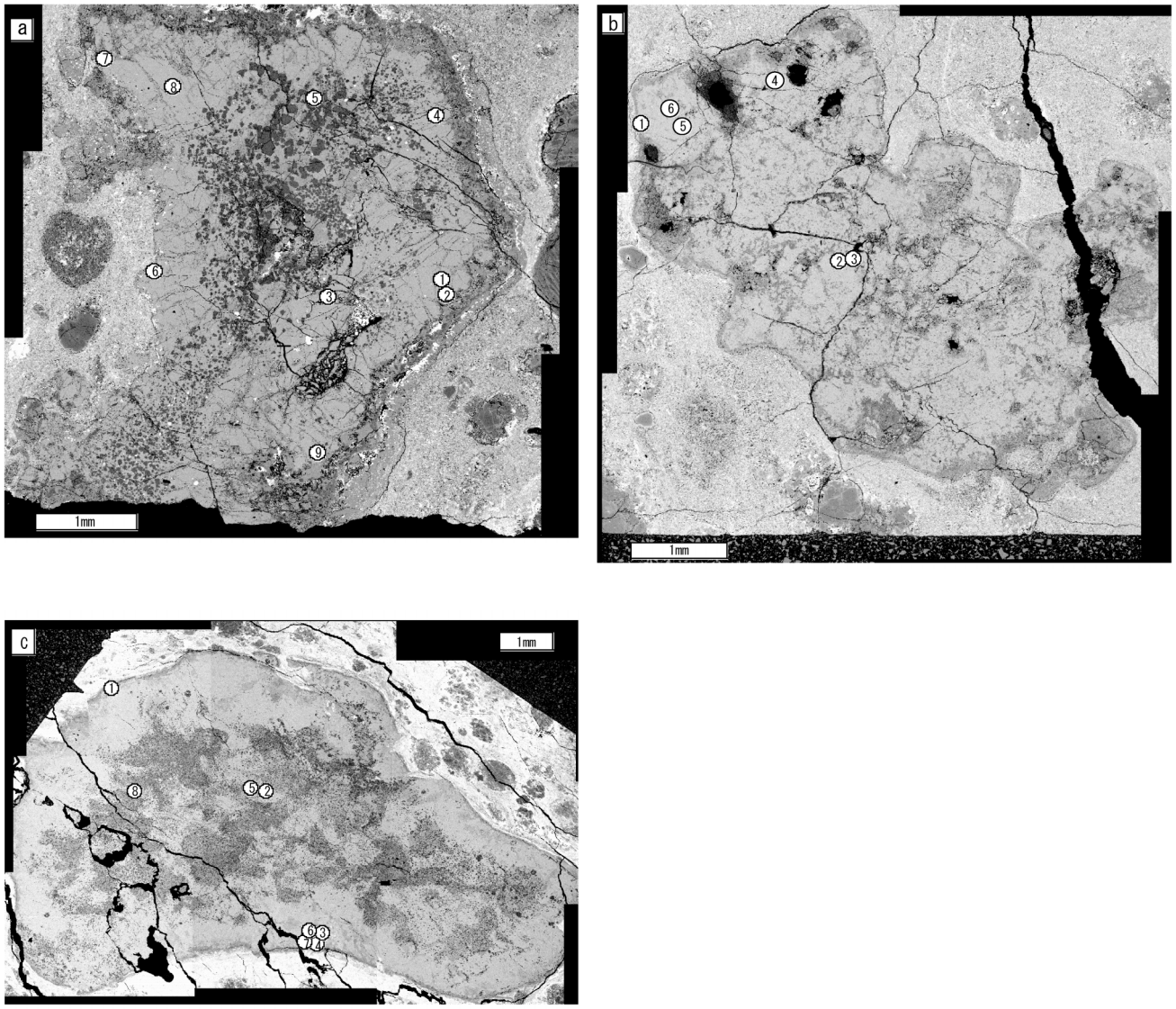

Fig. 1. Backscattered electron images of CAIs. a) AL-2. b) AL-9. c) SH-1. Circled numbers show locations of SIMS analyses. The numbers are given according to the order of SIMS measurements. In the CAIs, small darkest grains are spinel, and light-gray area is melilite. Some of the uniform black areas in the CAIs are filled with epoxy. Areas slightly darker than melilite are either fassaite, anorthite or altered areas containing Na etc.

EXPERIMENTAL

Samples

AL-2 is a type B CAI from Allende, ~5 mm in size with a well-developed melilite mantle and has a thick rim (Fig. 1a). Fassaite is abundant in the core of this CAI. Anorthite is present only near the rim, suggesting that it was formed by secondary alteration. Melilite compositions in AL-2 are normal for a type B CAI, ranging from Ak15 to Ak60. No large-scale systematic change in the melilite compositions from the core to the rim was observed in this CAI. This suggests that there were many nucleation sites for melilite crystals in the interior of the CAI and hence the CAI rim is not the dominant nucleation site.

AL-9 is also a CAI from Allende, ~5 mm in size and has a very irregular shape (Fig. 1b). Fassaite is mainly found in areas rich in spinel grains. Anorthite is present in the interior and also near the rim. Melilite in AL-9 is Al-rich (from Ak5 to Ak27) suggesting that this CAI may be akin to type A CAIs. No large-scale systematic change in the melilite compositions from the core to the rim was observed in this CAI.

SH-1 is a type B1 CAI from Sahara 98044 (CV3), ~1

cm in size with a well-developed melilite mantle (Fig. 1c). Fassaite and anorthite are present in the core and the mantle of this CAI. Melilite compositions in SH-1 are normal for type B CAIs, ranging from Ak20 to Ak43. In SH-1, melilite near the rim seems to be always Al-rich suggesting that the melilite grains nucleated at the surface of the CAI. But, no large-scale systematic change in the melilite compositions from the core to the rim was observed in this CAI.

Crystals of synthetic akermanite and gehlenite and glass samples of Ak50 and Ak30 compositions were used for calibration of composition dependence of isotopic fractionations measured by SIMS. These samples were produced in air to avoid isotopic fractionation.

Ion microprobe measurements

A Cameca IMS-6F ion probe at University of Tokyo was used for the measurements. Since instrumental isotopic fractionation could results from many factors, exactly the same measurement conditions are required for standards and CAI samples. Therefore, both a CAI and a standard sample (glass of Ak50 composition) were set in a polished section. Intrinsic isotope fractionations were obtained from the difference in isotopic compositions between the CAI and the standard sample.

In the case of CAI melilite samples and the accompanying Ak50 samples, both Mg and Si isotopes were measured on the same spot. Both Si and Mg isotopic fractionations were measured with the same ion probe setting except for the entrance slit width which was adjusted to give nearly the same count rates (1×10^5 c/s) of major isotopes. In the case of standard synthetic samples (gehlenite, glass(Ak50), glass(Ak30) and akermanite set together in a holder), Si and Mg measurements were made separately, mainly because comparison among the synthetic samples was the main aim of the measurements, and partly because the homogeneity of the isotopic compositions were guaranteed for these samples.

Since the absolute value of the Si instrumental mass fractionation is large (~–30 ‰/amu for melilite compared with –7 ‰/amu for Mg), reproducibility of the experimental conditions is important, particularly for Si isotope measurements. Our measurement conditions were chosen because they were easily reproducible. A defocused and intense $^{16}O^-$ primary beam (22.6 KeV, 35 micrometer in diameter; 1.6 nA) was used. The secondary ions (Mg^+ and Si^+ at 10 KeV) were extracted from the center of the sputtered area ~11 micrometer in diameter. Since the secondary ion signals were strong, this small aperture was used to reduce the signal to appropriate levels. In the secondary ion column, the energy slit was wide open (~100 eV) and the largest focal plane aperture (400 μm in diameter) was selected so that all secondary ions (with various energies and directions of movement) were evenly sampled. The entrance slit position was adjusted to maximize secondary ion signals. The mass resolving power was set to ~4000 which was enough for eliminating all significant interferences. The count rates for ^{24}Mg and ^{28}Si were set to ~1×10^5 c/s, so that slight changes in the dead time of the counting system do not affect the isotopic ratios significantly. Charge-up of sputtered area was detected by observing the secondary ion beam position on the focal plane and offset voltage was applied to compensate the charge-up effects. In the depth profile, Si^+ count rate showed complicated change during the first ~15 minutes of sputtering. First, a sharp peak in the counting rate was observed, then a minimum at ~1/2 of the peak count rate was observed. Then, another broad peak was observed before a steady count rate was achieved. Measurements were started after ~20 minutes of presputtering when secondary ion signals became steady. First Si isotopes were measured for 21 minutes then Mg isotopes were measured for 17 minutes.

The quasi-simultaneous arrival effects reported by Slodzian *et al*. (2001) need to be taken care of when measurements were made by a counting system based on an electron multiplier. The effect on the present measurements is probably small because molar fractions of Si and Mg in melilite are small (~0.1). Furthermore, since intrinsic mass fractionations were obtained from the differences between natural melilites and synthetic samples that were measured under practically identical conditions, the quasi-simultaneous arrival effects canceled out in the intrinsic mass fractionations.

Measurements were made at several locations (near the rim, in the mantle and in the core; see Fig. 1) in the CAIs. Al was measured together with Mg for Al-Mg age determination. The Al measurements were made with a Faraday cup whereas the Si and Mg measurements were made with an electron multiplier. The reference values for magnesium isotopic ratios ($^{25}Mg/^{24}Mg = 0.12663$ and $^{26}Mg/^{24}Mg = 0.13932$) are taken from Catanzaro *et al*. (1966). $\Delta^{25}Mg$ and $\Delta^{26}Mg$ are defined as differences from the reference values in ‰ unit. The reference values for Si have not been well established. For now we use the values ($^{29}Si/^{28}Si = 0.050633$ and $^{30}Si/^{28}Si = 0.033474$) reported by Zinner (1989). $\Delta^{29}Si$ and $\Delta^{30}Si$ are defined as differences from the reference values in ‰ unit. For this choice of reference Si isotopic ratios, measured Si isotopic compositions do not plot exactly on the mass fractionation line through the origin on the Si three isotope plot, but rather plot slightly below the mass fractionation line (see below). But this is not a problem in this study because we only discuss variations along a line of a slope 1/2.

Isotope fractionations of Si (hereafter $F(Si)$) were obtained by projecting the isotopic compositions ($\Delta^{29}Si$ and $\Delta^{30}Si$) onto the mass fractionation line of a slope 1/2

Table 1. Nominal (intrinsic + instrumental) Si and Mg isotope fractionations of synthetic samples

Sample	Mean F(Si) $\pm 2\sigma$ (‰/amu)	N*	$2\sigma_{mean}$ (‰/amu)	Mean F(Mg) $\pm 2\sigma$ (‰/amu)	N*	$2\sigma_{mean}$ (‰/amu)
Ak100	–32.7 ± 0.8	4	0.4	–6.1 ± 1.4	7	0.5
Ak50	–33.9 ± 1.0	4	0.5	–6.9 ± 1.4	12	0.4
Ak30	–33.4 ± 0.9	4	0.4	–6.9 ± 1.2	6	0.5
Gehlenite	–33.0 ± 1.4	2	1.0			

N = number of measurements.

on the three-isotope plot. (The slope of the fitting line to all the Si data (CAI and synthetic) of this study is 0.51 ± 0.07 (1σ). A more precise slope (0.501) has been obtained by Clayton *et al*. (1985). Because of the limited range of the Δ^{30}Si values (~12‰) in our data, a slight difference in the estimated slope does not make much difference in the Si fractionation values obtained by projection onto the fitting line.) Similarly, isotope fractionations of Mg (hereafter F(Mg)) of synthetic samples (akermanite, gehlenite, Ak30 glass and Ak50 glass set together in a holder) were obtained by projecting the isotopic compositions (Δ^{25}Mg and Δ^{26}Mg) onto the mass fractionation line. In the case of Mg in CAIs, because of the variable amounts of excess ^{26}Mg from ^{26}Al decay, such projection was not appropriate and Δ^{25}Mg value itself was used as F(Mg). (Also, in the case of Ak50 samples accompanying the CAIs, Δ^{25}Mg value itself was used as F(Mg) to avoid any systematic error due to different handling of the data between the CAIs and the standard samples.) The advantage of using values projected onto the mass fractionation line is reduced errors because errors in the direction perpendicular to the fractionation line can be ignored. Note that F values are nominal (intrinsic + instrumental) isotope fractionations relative to the reference values. Intrinsic mass fractionations were calculated from the differences in F values between the CAI and the standard sample. Excess ^{26}Mg due to ^{26}Al decay was calculated by $\delta^{26}\text{Mg} = \Delta^{26}\text{Mg} - 2 \times \Delta^{25}\text{Mg}$.

Three kinds of errors of isotopic ratios are discussed in the following sections. 2σ designates twice of standard deviation. This is used for 1) errors due to counting statistics for each measurement (e.g., errors of F values for one spot on CAI melilite) and 2) deviations around the mean value for repeated (N times) measurements (e.g., deviations of F values for several spots on CAI melilite). $2\sigma_{mean}$ designates twice of the estimated error of a mean value for repeated measurements, calculated by $2\sigma_{mean} = 2\sigma/N^{1/2}$. This indicates reliability of the estimated average value. Typical 2σ errors due to counting statistics for F(Si) are 0.8 ‰/amu. Typical 2σ errors due to counting statistics for F(Mg) in CAIs and synthetic samples are 1.1 ‰/amu and 0.5 ‰/amu, respectively.

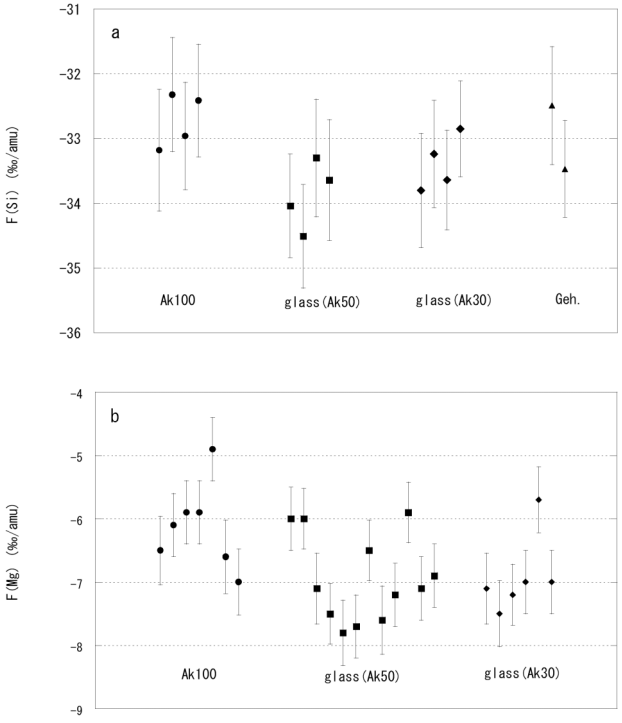

Fig. 2. (a) Si and (b) Mg isotope fractionations of synthetic samples (akermanite and gehlenite crystals and glass samples of Ak30 and Ak50 compositions) measured by SIMS. These are due to instrumental mass fractionation. Error bars are 2σ due to counting statistics. Nearly constant fractionations among these samples suggest that fractionations do not depend on the melilite composition.

RESULTS

The results of Si and Mg isotopic measurements of synthetic samples that were set in a holder and measured in a session under a virtually identical condition are summarized in Table 1. Figures 2a and 2b show that the isotopic fractionations of Si and Mg are nearly constant among these samples within the respective $2\sigma_{mean}$ values (~1.0 ‰/amu for Si and ~0.5 ‰/amu for Mg). In other words, matrix effects are not important among melilite

Table 2. Si and Mg isotopic compositions of CAIs and accompanying Ak50 samples

Sample*	F(Si) $\pm 2\sigma$** (‰/amu)	F(Mg) $\pm 2\sigma$** (‰/amu)	δ^{26}Mg $\pm 2\sigma$ (‰)	Al/^{24}Mg
AL-2				
mel-1	–33.0 ± 0.7	–0.3 ± 1.1	2.0 ± 2.4	6.8
mel-2	–34.2 ± 0.7	0.3 ± 1.1	1.5 ± 2.5	4.9
mel–3	–34.4 ± 0.7	–0.2 ± 1.1	2.2 ± 2.6	6.5
mel-4	–33.9 ± 0.8	–0.5 ± 1.3	4.6 ± 3.0	8.7
mel-5	–33.0 ± 0.7	–0.9 ± 1.1	2.3 ± 2.5	1.6
mel-6	–32.5 ± 0.8	–0.2 ± 1.5	4.2 ± 3.4	10.5
mel-7	–33.9 ± 0.7	1.2 ± 1.1	5.0 ± 2.6	8.9
mel-8	–33.6 ± 0.7	0.5 ± 1.1	1.8 ± 2.6	7.9
mel-9	–34.2 ± 0.7	0.1 ± 1.1	1.6 ± 2.6	7.6
Average (9)	–33.6 ± 1.3 (0.4)	0.3 ± 1.3 (0.4)	—	—
Ak50 (6)	–36.3 ± 0.9 (0.4)	–9.3 ± 1.8 (0.7)	—	—
AL-9				
mel-1	–34.5 ± 0.7	–6.0 ± 1.6	6.3 ± 3.8	26.8
mel-2	–36.8 ± 0.7	–5.0 ± 1.6	10.6 ± 3.7	30.5
mel–3	–36.2 ± 0.7	–3.7 ± 1.6	8.4 ± 3.8	28.3
mel-4	–36.7 ± 0.8	–6.0 ± 2.1	13.0 ± 4.8	49.2
mel-5	–36.9 ± 0.7	–4.3 ± 1.2	5.0 ± 2.8	14.2
mel-6	–34.3 ± 0.8	–4.8 ± 1.6	7.5 ± 3.8	23.9
Average (6)	–35.7 ± 2.4 (1.0)	–4.8 ± 1.9 (0.8)	—	—
Ak50 (7)	–36.4 ± 1.1 (0.4)	–9.4 ± 1.6 (0.5)	—	—
SH-1				
mel-1	–33.7 ± 0.7	–0.8 ± 1.2	3.5 ± 2.6	10.3
mel-2	–34.5 ± 0.8	–1.8 ± 1.1	2.2 ± 2.6	9.1
mel–3	–34.0 ± 0.7	–0.8 ± 1.1	–0.7 ± 2.7	4.1
mel-4	–32.0 ± 0.7	–1.2 ± 1.1	2.4 ± 2.5	9.8
mel-5	–33.2 ± 0.7	0.2 ± 1.1	0.1 ± 2.6	4.1
mel-6	–32.5 ± 0.7	–1.6 ± 1.0	4.6 ± 2.4	6.9
mel-7	–31.7 ± 0.7	–1.8 ± 1.1	4.8 ± 2.6	10.4
mel-8	–31.1 ± 0.7	0.0 ± 1.1	3.5 ± 2.7	4.6
Average (8)	–32.9 ± 2.4 (0.8)	–1.0 ± 1.5 (0.5)		
Ak50 (6)	–34.8 ± 1.3 (0.5)	–7.3 ± 2.8 (1.2)		

The 2σ error attached to each CAI datum is due to counting statistics.
**: Number of measurements is given in parenthesis.*
***: Values in these columns are nominal (intrinsic + instrumental) isotopic fractionations relative to reference values. $2\sigma_{mean}$ errors of the estimated mean values are given in parenthesis.*

samples. Thus isotopic fractionations in CAI melilites (after correcting for a standard melilite) are attributable to intrinsic fractionation (e.g., due to evaporation) rather than matrix effects.

The results for melilite in CAIs and accompanying Ak50 samples are summarized in Table 2. The sample numbers given in Table 2 correspond to the spots of SIMS analysis on the CAI shown in Fig. 1. Tables 1 and 2 show that the 2σ deviation of F(Si) for a synthetic sample is less than 1.4 ‰/amu (the largest deviation for gehlenite in Table 1). The 2σ of F(Mg) for a synthetic sample are less than 2.8 ‰/amu (the largest deviation for Ak50 accompanying SH-1 in Table 2). These deviations of the F values for a synthetic sample are somewhat larger than those expected from the counting statistics of each measurement. However, compared with the range of F(Si) ~ 5 ‰/amu errors reported by Hua *et al.* (2001a) for a synthetic sample, the present results seem more precise.

Four glass samples of Ak50 composition that were set (not intentionally) differently in SIMS holders, were measured in this study (Tables 1 and 2). The average F(Si) values (and $2\sigma_{mean}$) for individual glass samples range from –33.9 ± 0.5 to –36.4 ± 0.4 ‰/amu and the average F(Mg) values (and $2\sigma_{mean}$) range from –6.9 ± 0.4 to –9.4 ± 0.5 ‰/amu. These data show that the variations in the fractionations among the four samples cannot be accounted by statistical deviations. This means that significant instrumental mass fractionations occur among the

samples that were set in SIMS holders (not intentionally) differently. Thus, having a standard sample on the same polished section together with a CAI is quite important. We note in passing that the average F(Si) and the average F(Mg) are well correlated among the four Ak50 samples.

In one case (Ak50 measured with SH-1), the deviation of the Mg isotopic fractionation (2σ = 2.8 ‰/amu) was considerably larger (>5×) than that expected from counting statistics. Thus, there still remained some instrumental factors (other than setting of samples) that were not well controlled in the present measurements. Nevertheless, the errors are generally small enough for the purpose of this study. As will be shown later (Fig. 4c), in this Ak50 sample, F(Mg) seems to be correlated with F(Si).

As we mentioned already, the average F(Mg) for Ak50 glass samples set in different holders ranged from –6.9 to –9.4 ‰/amu. These values are quite similar to those reported by Fahey *et al*. (1987). But the agreement may be fortuitous because the data by Fahey *et al*. (1987) were obtained from the early stage of sputtering whereas our data were obtained after a long presputtering period. The instrumental Si isotope fractionation for Ak50 glass samples set in different holders ranged from –33.9 to –36.4 ‰/amu, as we mentioned already. This is quite different from that (–49.2 ‰/amu) reported by Fahey *et al*. (1987). Such a difference is not unexpected because instrumental mass fractionations depend on the setting of the ion microprobe (e.g., extraction voltage of secondary ions) quite sensitively.

Mg isotopic compositions in CAIs are positively fractionated relative to those in the Ak50 samples and are nearly constant within each CAI (Table 2).

The Si isotopic compositions of CAIs and accompanying Ak50 samples are shown in Fig. 3. On average, the data points are located below the fractionation line. This is probably due to the choice of the reference values of Si isotopic compositions that appear not well established (Zinner, 1989). F(Si) and F(Mg) in CAIs and accompanying Ak50 samples are shown in Fig. 4. Figure 4 shows that deviations of F(Si) and F(Mg) within a CAI are not very large (≤2.4 ‰/amu for Si and ≤1.9 ‰/amu for Mg). In particular, in the case of AL-2, 2σ deviations of F(Si) and F(Mg) are both only ~1.3 ‰/amu. But the 2σ deviations of Si isotope fractionations for AL-9 and SH-1 are ~2.4 ‰/amu, noticeably larger than that ~0.8 ‰/amu expected from counting statistics. These deviations of Si isotopic fractionations could be due to intrinsic fractionation within the CAIs. But in view of the example (Fig. 4c) that a 2σ deviation that is larger than that expected by counting statistics could happen even for a standard sample, we consider that these deviations of fractionations are due to variable instrumental fractionation.

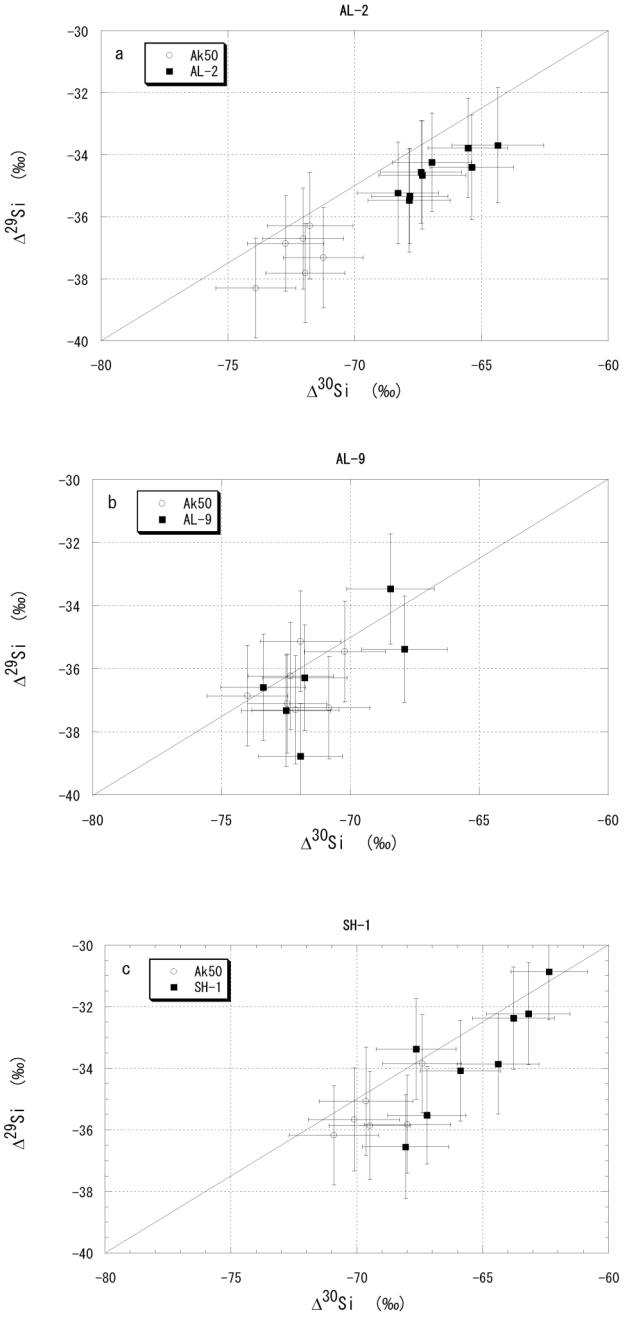

Fig. 3. Nominal (intrinsic + instrumental) Si isotope fractionation in (a) AL-2 and the accompanying Ak50 glass, (b) AL-9 and the accompanying Ak50 glass and (c) SH-1 and the accompanying Ak50 glass. In all cases, data points tend to be plotted slightly below the fractionation line passing through the reference value of Si (Zinner, 1989). Deviations of Si data points for AL-9 and SH-1 are considerably larger than those expected from counting statistics. However, based on a couple of lines of evidence we argue that these deviations could be due to instrumental fractionations.

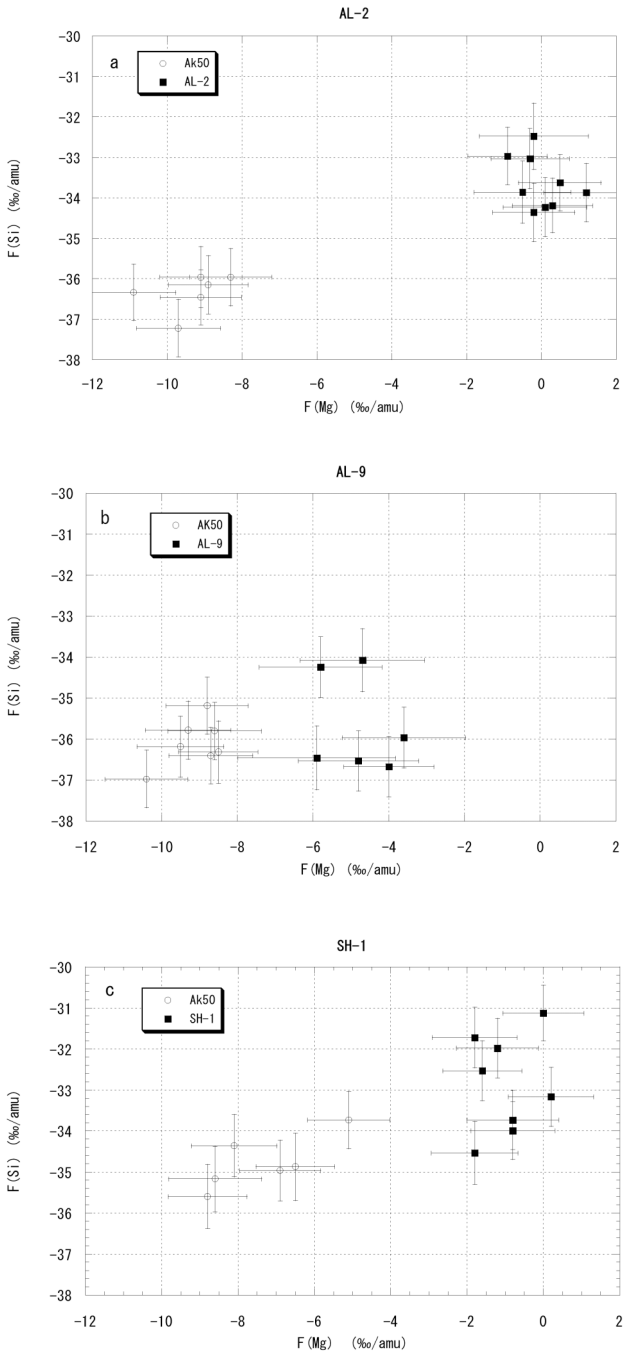

Fig. 4. Nominal (intrinsic + instrumental) isotopic fractionations of Si and Mg in (a) AL-2 and the accompanying Ak50 glass, (b) AL-9 and the accompanying Ak50 glass and (c) SH-1 and the accompanying Ak50 glass. The deviations in F(Si) and F(Mg) are not well correlated in AL-9 and SH-1. Also note a relatively large deviation of F(Mg) for Ak50 accompanying SH-1. This deviation is due to instrumental fractionation.

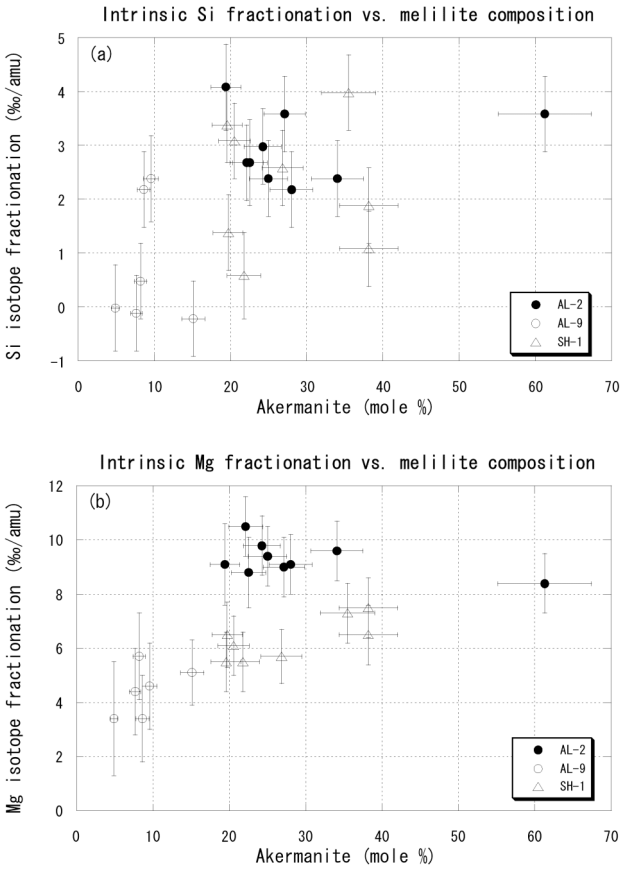

Fig. 5. Intrinsic isotopic fractionations of (a) Si and (b) Mg plotted against akermanite mole %. In both figures isotope fractionations do not show significant dependence on akermanite content. F(Si) values have been adjusted assuming –0.28 ‰/amu for terrestrial samples.

There are a couple of lines of evidence that support this view.

1) F(Si) values at nearby spots are not well correlated. For instance, in the case of AL-9, F(Si) = –36.9‰ of spot #5 was the lowest value but a nearby spot #6 gave the highest value of F(Si) = –34.3‰.

2) Also, there appear to be no significant differences in the Si and Mg isotopic compositions at different locations of CAIs (core, mantle and near the rim). For instance, the highest F(Si) value in SH-1 was observed in the core (spot #8) whereas the second highest value was observed near the rim (spot #7).

3) The F(Si) within a CAI is not correlated with the F(Mg) (Fig. 4). Since F(Si) and F(Mg) should be correlated if the fractionations resulted from vaporization, this suggests that the deviations in the F(Si) in AL-9 and SH-1 are not due to intrinsic fractionation. Also, no correlation between the melilite composition and the isotope

Table 3. Intrinsic Si and Mg isotope fractionations and inferred initial $^{26}Al/^{27}Al$ in CAIs

Sample	Si* (‰/amu)	Mg* (‰/amu)	$(^{26}Al/^{27}Al)_0$
AL-2	2.9 ± 1.6 (0.6)	9.6 ± 2.1 (0.8)	(3.8 ± 1.7) E-05
AL-9	1.0 ± 2.6 (1.1)	4.6 ± 2.5 (0.9)	(3.6 ± 0.7) E-05
SH-1	2.2 ± 2.7 (1.0)	6.4 ± 3.2 (1.3)	(5.3 ± 2.3) E-05

**: Errors represent 2σ deviations. $2\sigma_{mean}$ errors of the mean values are given in parenthesis.*
Uncertainties of the isotopic compositions of synthetic samples (~0.3 ‰/amu for Si and ~2 ‰/amu for Mg) are not propagated to the errors shown in this table.

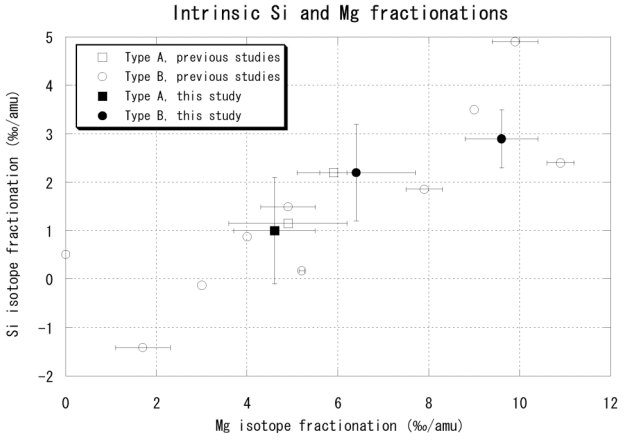

Fig. 6. Relationship between average intrinsic isotopic fractionation of Mg and Si for three CAIs obtained by SIMS in this study together with literature data (Grossman et al., 2000). The Si fractionation values of both literature data and the present data are shifted upward by 0.28 ‰/amu.

fractionations was observed (see Fig. 5 and $Al/^{24}Mg$ in Table 2).

Thus we consider that both Si and Mg isotopic compositions within each CAI are essentially constant for all three CAIs studied here. Although, detailed documentation of Si- and Mg-isotopic homogeneity of CAIs were scarce, it is possible that a majority of CAIs have homogeneous isotopic compositions. If, in spite of the above argument, the 2σ deviations of F values within a CAI are intrinsic, then the data in Table 2 suggest that the intrinsic deviations (2σ) of up to 2.4 ‰/amu for Si and up to 1.9 ‰/amu for Mg are present in the CAIs.

From the differences in the average isotopic compositions between CAIs and the accompanying Ak50 samples, intrinsic isotope fractionations of Si and Mg were calculated (Table 3). We do not know the exact isotopic compositions of the synthetic samples. In the case of Si, meteorites and terrestrial samples seem to be generally

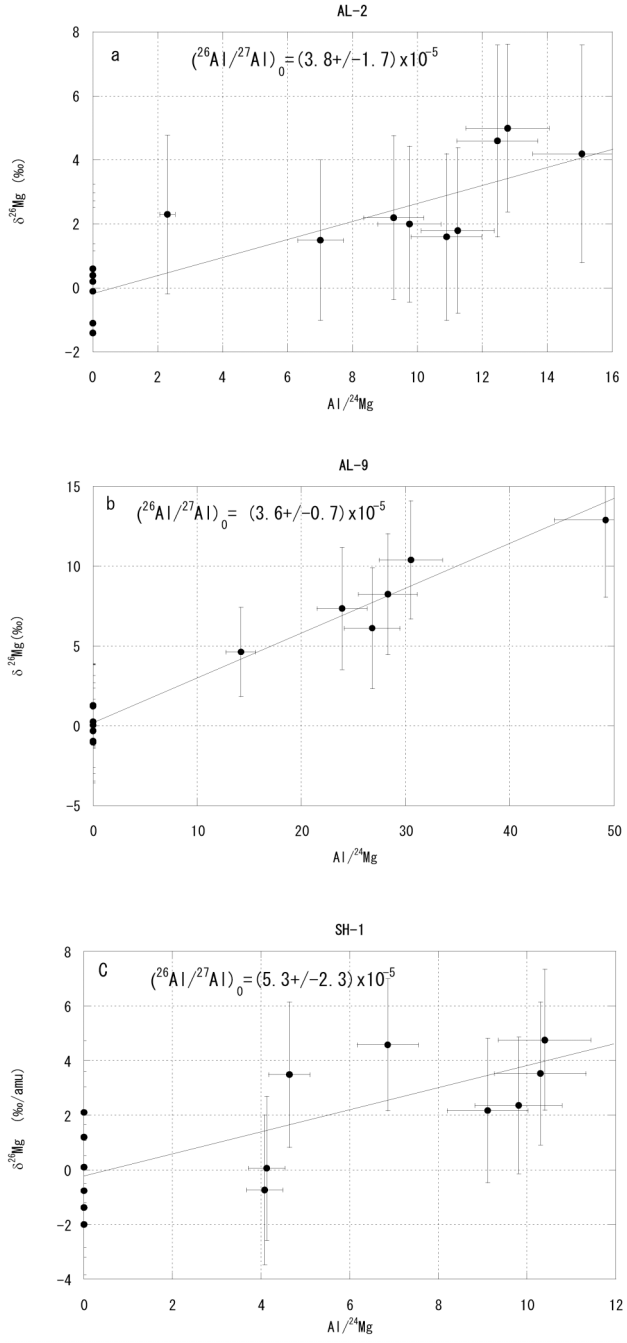

Fig. 7. Al-Mg systematics in (a) AL-2, (b) AL-9 and (c) SH-1. Data from synthetic glass samples are plotted on the y-axis.

fractionated by ~–0.28 ‰/amu relative to the reference value (Grossman *et al.*, 2000). Therefore, Si isotopic data of CAIs discussed in Grossman *et al.* (2000) were adjusted upward by 0.28 ‰/amu. We also assumed this –0.28 ‰/amu for our synthetic samples. The uncertainty of the Si isotopic fractionation in our synthetic samples may be ~0.3 ‰/amu.

In the case of Mg, natural terrestrial materials seem to have well restricted isotopic compositions (Catanzaro and Murphy, 1966). But synthetic metallic Mg seems to have larger mass fractionations (Galy *et al*., 2001). We assumed 0.0 ‰/amu for the Mg isotope fractionation in our synthetic samples. According to the literature values of Mg isotopic composition in terrestrial materials (Catanzaro and Murphy, 1966; Galy *et al*., 2001) the uncertainty of Mg isotopic fractionation in our synthetic samples may be as large as 2 ‰/amu.

As shown in Fig. 6, Si and Mg in these CAIs are isotopically heavy and Si and Mg fractionations are correlated. It can be seen that the isotopic fractionations obtained by SIMS in this study agree quite well with literature values obtained by bulk analyses.

Inferred initial $^{26}Al/^{27}Al$ values of the CAIs are given in Table 3. Al-Mg isochron diagrams for melilite of the three CAIs are shown in Fig. 7. The isochron was fairly well determined for AL-9 because of low-Mg concentrations in the melilite. Precisions of the inferred $^{26}Al/^{27}Al$ ratios for AL-2 and SH-1 are not as good due to the limited ranges in the $Al/^{24}Mg$ ratios. The inferred $^{26}Al/^{27}Al$ ratios in melilite in these CAIs are nearly identical with the canonical value (5×10^{-5}) within the 2σ errors (Table 3).

Discussion

Si and Mg in the three CAIs are isotopically heavy, suggesting that these CAIs experienced evaporative loss of these elements. The average Si and Mg isotope fractionations for each CAI are positively correlated and agree well with those obtained by analyses of bulk CAIs (Clayton *et al*., 1988). Si and Mg isotope fractionations resulting from evaporative loss of Si and Mg from high-temperature condensates were studied in detail by Grossman *et al*. (2000). The isotopic fractionations of Si and Mg in the present CAIs correspond to losses of 5–20% of Si and 20–40% of Mg.

The model of Grossman *et al*. (2000) predicted that type A inclusions should record smaller Si isotope fractionations than type B inclusions for a given amount of Mg isotope fractionation. So far, such a difference in Si isotope fractionations between type A and type B inclusions has not been observed. Certainly, more isotopic data are needed to find out if there are significant isotopic differences between type A and type B inclusions.

Grossman *et al*. (2002) presented an advanced model of formation of coarse-grained CAIs, by incorporating cooling history of a CAI melt. Assuming that the CAI melt continued to evaporate during the cooling stage of the CAI formation, it was predicted that late-forming melilite (which is Mg-rich) should have more fractionated Si and Mg isotopic compositions. (Note that in this model, melt is assumed to be homogeneous.) According to this model, Mg isotope fractionations in a CAI range from a couple of ‰/amu to more than 10 ‰/amu, depending on various parameters. The present study, however, showed that the Si and Mg isotopic compositions are nearly constant within each CAI, and no correlation between the melilite composition and the isotope fractionations was observed (Fig. 5 and $Al/^{24}Mg$ in Table 2). In particular, it seems not possible to produce unzoned fractionation of F(Mg) and F(Si) observed in AL-2 by the model of Grossman *et al*. (2002).

A possible explanation for this isotopic homogeneity within each CAI may be reduction of the surface area of melt during cooling of CAIs. As already discussed by Grossman *et al*. (2002), the surface of CAI melt may be covered with solid spinel and/or melilite, which prevents further evaporation from the melt.

Another possible explanation for the isotopic homogeneity of CAIs provided by Grossman *et al*. (2002) was multiple melting events experienced by CAIs. The argument is based on high Na concentrations in some CAIs (MacPherson and Davis, 1993). Since a significant amount of Na is not expected to remain in a melt from which ~20% of Si and Mg evaporated, it was suggested that Si and Mg isotope fractionations may have been established in an earlier melting event before incorporation of Na. MacPherson and Davis (1993) showed that in a remelted CAI, Na and Mg concentrations show a good correlation due to fractional crystallization. We examined present CAIs for remelting signature and did not find good evidence for it. Na concentrations in the melilite were not very high and did not correlate with Mg concentrations but seem to be relatively high in areas near alteration products. Thus, present CAIs are considered not to have been remelted.

Another possible explanation for the isotopic homogeneity of CAIs that cannot be, a priori, ruled out, is isotope homogenization by later metamorphic events. However, ^{26}Mg heterogeneity is preserved in the melilite in these CAIs (Fig. 7). Also, Mg self-diffusion is expected to be as slow as the MgSi-AlAl inter-diffusion in melilite (Morioka and Nagasawa, 1991). Since chemical heterogeneity of melilite is well preserved in melilite in the CAIs, it is unlikely that the constant isotopic fractionations in the CAIs resulted from metamorphic events.

Thus, we consider that reduced surface area of liquid during cooling of CAIs is the most plausible explanation for the lack of zoning of isotopic compositions in these CAIs. In contrast to these CAIs, a couple of CAIs are known to have isotope zoning, lighter isotopic compositions in the interior and heavier isotopic compositions in the region near the rim (E40 studied by Goswami *et al*., 1994; Vigarano 1623-5 studied by Davis *et al*., 1991).

Such zoning may be explained by the model of Richter *et al*. (2002). In this model, depending on the choice of the parameters, evaporation of Mg and Si could be very fast compared with diffusion of these elements in the melt, resulting in both compositional and isotopic zoning in the melt. (This is in contrast with the model of Grossman *et al*. (2002) where the melt is always homogeneous both compositionally and isotopically.) Goswami *et al*. (1994) showed that the melilite in the CAI (E40) is both compositionally and isotopically zoned from the rim to the interior. In contrast, no large scale zoning of the melilite composition from the rim to the core across the melilite mantle was observed in the present CAIs.

Quick evaporation of Si and Mg is possible under a high ambient H_2 pressure. Under lower H_2 pressures, evaporation is slow and it is possible to have nearly homogeneous isotopic and chemical compositions in the melt by diffusive homogenization. According to Richter *et al*. (2002), the absence of isotopic zoning in the present CAIs suggests that H_2 pressure was less than $\sim 10^{-4}$ bars during the heating event. During cooling of CAIs, surface area of liquid may be reduced by formation of solid spinel and/or melilite, preventing further evaporation and isotope fractionation in late crystallizing melilite. The model of Richter *et al*. (2002) is attractive in the sense that both isotopic homogeneity and heterogeneity can be explained by adopting different ambient H_2 pressures. The Al-Mg ages of these CAIs suggest that the Mg isotopic fractionation was established when the coarse-grained CAIs were initially formed.

Conclusions

Si and Mg isotopic compositions in melilite in synthetic samples and three coarse-grained CAIs were measured. The isotopic fractionations of Si and Mg measured by SIMS are nearly constant for the synthetic melilite samples. Thus isotopic fractionations in CAI melilite (after correcting for a standard melilite) are attributable to intrinsic fractionation (e.g., due to evaporation) rather than matrix effects.

Si and Mg in the three CAIs are isotopically heavy and the isotope fractionations are fairly well correlated, suggesting that these CAIs experienced evaporative loss of these elements. The average Si and Mg isotopic fractionations in each CAI fit well in the range obtained by bulk measurements (Clayton *et al*., 1988). These isotopic compositions are well explained by the model of Grossman *et al*. (2000) where coarse-grained CAIs were formed by heating high-temperature condensates.

The Si and Mg isotopic compositions of melilite are virtually constant within each CAI studied here. In contrast, there are a couple of CAIs that were reported to show isotopic zoning. These disparate observations suggest that H_2 partial pressure was variable either spatially or temporally during formation of coarse-grained CAIs.

Acknowledgments—Synthetic samples of akermanite and gehlenite were kindly provided by Dr. M. Morioka. The authors thank Drs. T. Kunihiro and F. Richter for constructive comments.

References

Catanzaro, E. J. and Murphy, T. J. (1966) Magnesium isotope ratios in natural samples. *J. Geophys. Res.* **71**, 1271–1274.

Catanzaro, E. J., Murphy, T. J., Garner, E. L. and Shields, W. R. (1966) Absolute isotope abundance ratios and atomic weights of magnesium. *J. Res. Nat. Bur. Stand.* **70a**, 453–458.

Clayton, R. N., MacPherson, G. J., Hutcheon, I. D., Davis, A. M., Grossman, L., Mayeda, T. K., Molini-Velsko, C. and El Goresy, A. (1984) Two forsterite-bearing FUN inclusions in the Allende meteorite. *Geochim. Cosmochim. Acta* **48**, 535–548.

Clayton, R. N., Mayeda, T. K. and Molini-Velsko, C. A. (1985) Isotopic variations in solar system material: Evaporation and condensation of silicates. *Protostars & Planets II* (Black, D. C. and Matthews, M. S., eds.), 755–771, Univ. of Arizona Press.

Clayton, R. N., Hinton, R. W. and Davis, A. M. (1988) Isotopic variations in the rock-forming elements in meteorites. *Phil. Trans. R. Soc. Lond.* **A325**, 483–501.

Davis, A. M., Hashimoto, A., Clayton, R. N. and Mayeda, T. K. (1990) Isotope mass fractionation during evaporation of Mg_2SiO_4. *Nature* **347**, 655–658.

Davis, A. M., MacPherson, G. J., Clayton, R. N., Mayeda, T. K., Sylvester, P. J., Grossman, L., Hinton, R. W. and Laughlin, J. R. (1991) Melt solidification and late-stage evaporation in the evolution of a FUN inclusion from the Vigarano C3V chondrite. *Geochim. Cosmochim. Acta* **55**, 621–637.

Fahey, A. J., Zinner, E. K., Crozaz, G. and Kornacki, A. S. (1987) Microdistribution of Mg isotopes and REE abundances in a Type A calcium-aluminum-rich inclusion from Efremovka. *Geochim. Cosmochim. Acta* **51**, 3215–3229.

Galy, A., Belshaw, N. S., Kalicz, L. and O'Nions, R. K. (2001) High precision measurement of magnesium isotopes by multiple-collector inductively coupled plasma mass spectrometry. *Int. J. Mass Spectrom.* **208**, 89–98.

Goswami, J. N., Srinivasan, G. and Ulyanov, A. A. (1994) Ion probe studies of Efremovka CAIs: I. Magnesium isotope compositions. *Geochim. Cosmochim. Acta* **58**, 431–447.

Grossman, L., Ebel, D. S., Simon, S. B., Davis, A. M., Richter, F. M. and Parsad, N. M. (2000) Major element chemical and isotopic compositions of refractory inclusions in C3 chondrites: The separate roles of condensation and evaporation. *Geochim. Cosmochim. Acta* **64**, 2879–2894.

Grossman, L., Ebel, D. S. and Simon, S. B. (2002) Formation of refractory inclusions by evaporation of condensate precursors. *Geochim. Cosmochim. Acta* **66**, 145–161.

Hua, X., Wang, J. and Buseck, P. R. (2000) Silicon-isotopic

abundances in silicate minerals from the Kaba and Mokoia CV3 carbonaceous chondrites. *Meteoritics & Planetary Sci*. **35**, A78.

Hua, X., Huss, G. R. and Sharp, T. G. (2001a) SIMS measurements of silicon isotopic fractionation in olivine from the Kaba CV3 chondrite. *Meteoritics & Planetary Sci*. **36**, A85.

Hua, X., Wang, J., Huss, G. R., Sharp, T. G. and Buseck, P. R. (2001b) Si-isotopic fractionation in silicate minerals from chondritic meteorites: A possible new probe for early solar system processes. *32nd Lunar and Planetary Science Conference*, #1852.

Kennedy, A. K., Beckett, J. R., Edwards, D. A. and Hutcheon, I. D. (1997) Trace element disequilibria and magnesium isotope heterogeneity in 3655A: Evidence for a complex multi-stage evolution of a typical Allende Type B1 CAI. *Geochim. Cosmochim. Acta* **61**, 1541–1561.

MacPherson, G. J. and Davis, A. M. (1993) A petrologic and ion microprobe study of a Vigarano Type B refractory inclusion: Evolution by multiple stages of alteration and melting. *Geochim. Cosmochim. Acta* **57**, 231–243.

MacPherson, G. J., Crozaz, G. and Lundberg, L. L. (1989) The evolution of a complex type B Allende inclusion: An ion microprobe trace element study. *Geochim. Cosmochim. Acta* **53**, 2413–2427.

Morioka, M. and Nagasawa, H. (1991) Diffusion in single crystals of melilite: II. Cations. *Geochim. Cosmochim. Acta* **55**, 751–759.

Richter, F. M., Davis, A. M., Ebel, D. S. and Hashimoto, A. (2002) Elemental and isotopic fractionation of type B calcium-, aluminum-rich inclusions: Experiments, theoretical considerations, and constraints on their thermal evolution. *Geochim. Cosmochim. Acta* **66**, 521–540.

Slodzian, G., Chaintreau, R., Dennebouy, R. and Rousse, A. (2001) Precise in situ measurements of isotopic abundances with pulse counting of sputtered ions. *Eur. Phys. J.* **AP14**, 199–231.

Zinner, E. (1989) Isotopic measurements with the ion microprobe. New frontiers in stable isotopic research: Laser probes, ion probes and small-sample analysis. *U.S. Geol. Surv. B* **1890**, 145–162.